Phonon-assisted carrier tunneling with hyperfine-induced spin flip in coupled quantum dot systems

Paweł Karwat,[1,2] Krzysztof Gawarecki,[2] and Paweł Machnikowski [2]

[1]*School of Physics and CRANN Institute, Trinity College Dublin, Dublin 2, Ireland*
[2]*Department of Theoretical Physics, Wrocław University of Science and Technology, 50-370 Wrocław, Poland*

We calculate the rates of phonon-assisted hyperfine spin flips during electron and hole tunneling between quantum dots in a self-assembled quantum dot molecule. We show that the hyperfine process dominates over the spin-orbit-induced spin relaxation in magnetic fields up to a few teslas for electrons, while for holes this crossover takes place at field magnitudes of a fraction of a tesla, upon the assumption of a large d-shell admixture to the valence band state, resulting in a strong transverse hyperfine coupling. The interplay of the two spin-flip mechanisms leads to a minimum of the spin-flip probability, which is, in principle, experimentally measurable and can be used as a test for the presence of substantial transverse hyperfine couplings in the valence band.

DOI: 10.1103/PhysRevB.104.045308

I. INTRODUCTION

Hyperfine (hf) coupling between carrier spins and nuclear magnetic moments in a crystal [1] is one of the key factors determining the properties of semiconductor structures, such as quantum dots (QDs), and their usability in new information processing devices. Once considered the main source of dephasing [2–6], it can now be controlled with growing precision and used as a manageable degree of freedom [7–9].

The hf coupling for electrons is dominated by the approximately isotropic contact interaction. Its transverse components can, in principle, lead to spin relaxation accompanied by a simultaneous change in one of the nuclear spins (a "flip-flop" process). Due to a large mismatch between electronic and nuclear Zeeman energies, this process is restricted to very low magnetic fields [10–12] or bright-dark exciton resonances [13]. At magnetic fields exceeding a fraction of a tesla the hf processes become ineffective [14,15]. Even though the energy gap can be closed by emitting a phonon [16], it turns out that processes relying on the spin-orbit (SO) coupling dominate in this regime [17,18] due to their more favorable dependence on the magnetic field. A crossover between the hf and SO regimes has been observed in gated GaAs QDs [19].

Theoretical description of hf-induced spin flips was developed in the context of electrons in gated QDs [20,21]: One considers corrections to the carrier state with a given spin, mediated by the hyperfine coupling with all the nuclei, treated as a perturbation. In this way, the original state gets an admixture of inverted spin, which allows transitions to a state with a nominally opposite spin via spin-conserving phonon couplings. For a transition within the Zeeman doublet, the combination of the $\propto B^{-2}$ scaling of the hf admixture (stemming from the carrier Zeeman energy, while the nuclear Zeeman splitting is negligible), frequency dependence of the phonon spectral density, and Van Vleck cancellation leads to a $\propto B^3$ dependence on the magnetic field.

In the case of holes the physics of hf interactions is more complex, and some questions seem to remain open. Overall, the hole hf coupling is due to dipole interactions, which renders it much weaker than the contact interaction of electrons [22–24]. Moreover, for a purely p-type valence band, the transverse components of the hole hf coupling can result from only weak band-mixing effects [10,22,23], which would strongly limit hole spin relaxation. Indeed, a coherent population trapping experiment under transverse nuclear spin polarization in a low-noise device [25] has led to the conclusion that the transverse hyperfine coupling is negligible. On the other hand, selective measurements of the Overhauser field for particular elements and isotopes in the crystal [26] yield results that can be explained by a substantial admixture of atomic d-shell states to the valence band, in line with earlier theoretical calculations [27]. According to theoretical models, a d-shell admixture would give rise to a substantial transverse contribution to the hole hyperfine coupling [28]. Such a transverse component not only affects the dynamics of spin dephasing but also leads to efficient hf-induced hole spin relaxation.

In quantum dot molecules (QDMs), built of two coupled QDs, even in the s shell, spin relaxation not only can take place between states within one Zeeman doublet but can also accompany charge relaxation (dissipative tunneling) between the QDs. Such processes were extensively studied for two-electron configurations in the Pauli blockade regime of gated QDMs [29], where the spin-flip rates were determined experimentally [30]. Understanding the role of hyperfine interactions in such a carrier tunneling process may be important for possible spin injection schemes as well as for spin readout protocols involving carrier transfer induced by gating pulses. On the other hand, hf flip-flops combined with spatiotemporal dynamics of the carrier may be used to imprint a particular state in the nuclear system. Finally, theoretically predicted characteristics of the spin relaxation, when confronted with

the experiment, may verify the assumptions of the model and thus offer information on the nature of the hf coupling itself.

A reliable description of processes involving tunneling in self-assembled QD systems requires reasonable knowledge of wave functions, which is achievable with the $\boldsymbol{k} \cdot \boldsymbol{p}$ method in the envelope function approximation [31]. The $\boldsymbol{k} \cdot \boldsymbol{p}$ method allows one also to describe all kinds of phonon-assisted processes, including those involving SO-induced spin flips [32]. Recently, we also combined the $\boldsymbol{k} \cdot \boldsymbol{p}$ model with the hyperfine Hamiltonian and provided a description of hyperfine couplings based on multiband wave functions [28].

In this paper we calculate the rates of phonon-assisted hyperfine spin flip-flops during electron and hole relaxation between the two branches of the s shell in a QDM (corresponding to states localized in two different QDs if the system is away from the resonance). We compare the result with the SO-induced phonon-assisted spin-flip tunneling and show that the hyperfine process dominates for fields below a few teslas for electrons (depending on the axial electric field), while for holes it becomes important only for fields roughly below 0.1 T. The interplay of hf and SO mechanisms of spin relaxation leads to a nonmonotonic dependence of the total spin-flip probability, which may be used as a test for considerable transverse hyperfine couplings.

This paper is organized as follows. In Sec. II we describe the model of the system under study. Section III presents the theory for the phonon-assisted tunneling of a carrier with a simultaneous spin flip-flop between the carrier and a nuclear spin. In Sec. IV we present the results. Section V concludes the paper.

II. MODEL

We consider two coupled, vertically stacked self-assembled InGaAs quantum dots [Fig. 1(a)]. The dots are placed on wetting layers $a_G = 0.565325$ nm thick of In$_{0.4}$Ga$_{0.6}$As composition. The shape of each dot is defined by the restriction of its upper limit by the surface [33]

$$S_n(\boldsymbol{r}) = z_n^{(\mathrm{WL})} + h_n \exp\left(-\frac{(x^2 + y^2)^2}{r_n^4}\right),$$

where $n = \{1, 2\}$ refers to the bottom and top dots, respectively, $z_n^{(\mathrm{WL})}$ denotes the top of the wetting layer, h_n is the dot height, and r_n defines the lateral extension. We take approximately (subject to discretization) $h_1 = 4.8$ nm, $h_2 = 5.4$ nm, $r_1 = 15.8$ nm, and $r_2 = 17$ nm. Both dots have a trumpet-shaped composition [34], where the position-dependent In content is given by

$$C(\boldsymbol{r}) = C_{\mathrm{b}} + (C_{\mathrm{t}} - C_{\mathrm{b}}) \exp\left(\frac{-\sqrt{x^2 + y^2} \exp(-z/z_{\mathrm{c}})}{r_{\mathrm{c}}}\right),$$

where $C_{\mathrm{t}} = 0.7$ and $C_{\mathrm{b}} = 0.4$ are related to the compositions in the top and bottom regions of a given QD, $z_{\mathrm{c}} = 1.1$ nm, and $r_{\mathrm{c}} = 2.3$ nm. To simulate material intermixing, the dots are processed by a Gaussian blur with a standard deviation of 0.6 nm. The computations were carried out on $(200 \times 200 \times 200)a_G$ and $(100 \times 100 \times 70)a_G$ computational boxes for calculation of strain and electron states, respectively.
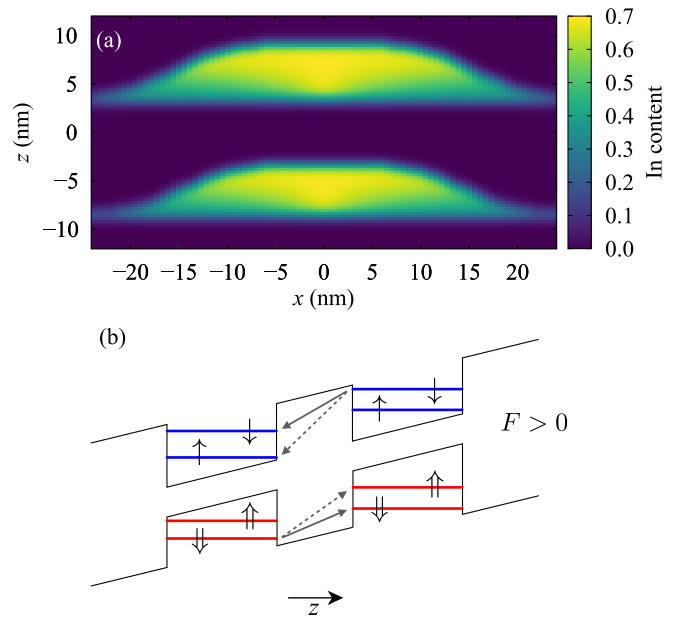

FIG. 1. (a) Material distribution in the system and (b) the scheme of the lowest energy levels, with spin-conserving and spin-flip transitions marked by solid and dashed grey arrows, respectively.

In order to quantitatively account for the hyperfine interactions in an inhomogeneous system like a QD, one needs to model the properties of wave functions on the mesoscopic scale of several or tens of nanometers and simultaneously describe the properties of Bloch functions near the nuclei on a subnanometer scale. No single computational method is currently able to bridge these two scales; hence, we use the hybrid approach developed in Ref. [28], in which the mesoscopic scale is covered by an eight-band $\boldsymbol{k} \cdot \boldsymbol{p}$ theory in the virtual crystal approximation, while the atomic-scale properties are approximately accounted for by a simple model of effective rescaled hydrogenlike orbitals with averaging over specific alloying and isotope configurations.

Thus, on the mesoscopic scale, the static strain related to the lattice mismatch is accounted for within the continuous elasticity approach [35]. The strain-induced piezoelectric potential is calculated including polarization up to the second order in strain tensor elements [36] with parameters from Ref. [37]. The wave functions for the four lowest electron and hole states (corresponding to the two QDs and two spin orientations are obtained using the eight-band $\boldsymbol{k} \cdot \boldsymbol{p}$ theory in the envelope function approximation. The Hamiltonian, the material parameters, and implementation are given in great detail in Ref. [38]. We also used improvements of the model described in Ref. [39].

The hyperfine Hamiltonian for the interaction of a carrier with nuclear spins is

$$H_{\mathrm{hf}} = 3E_{\mathrm{hf}} \sum_{\alpha} \zeta_{\alpha} \boldsymbol{A}(\boldsymbol{r} - \boldsymbol{R}_{\alpha}) \cdot \boldsymbol{I}_{\alpha}/\hbar, \tag{1}$$

where α labels the ions, $\boldsymbol{R}_{\alpha}$ are their positions,

$$E_{\mathrm{hf}} = \frac{2\mu_0}{3\pi} \mu_{\mathrm{B}} \mu_{\mathrm{N}} a_{\mathrm{B}}^{-3} = 0.5253 \, \mu\mathrm{eV},$$

μ_B and μ_N are Bohr and nuclear magnetons, respectively, a_B is the Bohr radius, μ_0 is the vacuum permeability, $\boldsymbol{I}_\alpha$ is the nuclear spin, ζ_α defines the nuclear magnetic moment for a given nucleus via $\boldsymbol{\mu}_\alpha = \zeta_\alpha \mu_N \boldsymbol{I}_\alpha$, and

$$A(r) = \frac{a_B^3}{4\hbar}\left[\frac{8\pi}{3}\delta(r)\boldsymbol{S} + \frac{\boldsymbol{L}}{r^3} + \frac{3(\hat{\boldsymbol{r}}\cdot\boldsymbol{S})\hat{\boldsymbol{r}} - \boldsymbol{S}}{r^3}\right]. \quad (2)$$

We consider the two most common In isotopes, two Ga isotopes, and one As isotope with angular momenta $j = 9/2$, $3/2$, and $3/2$, respectively. We neglect any effects of nuclear quadrupole couplings [40,41].

The Bloch function is modeled as a sum of atomic orbitals corresponding to the outermost shells, centered around the two nuclei in the primitive cell. The atomic orbitals are taken as hydrogenlike wave functions $\psi_{nlm}(\boldsymbol{r}) = \sqrt{n\xi_{nl}}\,\psi_{nlm}^{(H)}(n\xi_{nl}\boldsymbol{r})$, where $\psi_{nlm}^{(H)}(\boldsymbol{r})$ are the wave functions of the hydrogen atom and ξ_{nl} is a scaling parameter. Since only one shell of a given symmetry is relevant for the topmost valence and lowest conduction bands, the principal quantum number n will be omitted. The conduction band of zinc-blende crystals is commonly assumed to be built of atomic s states ($l = 0$), while the valence band is made of p states ($l = 1$), with the heavy-hole subband composed of states with $\pm 3/2$ projections of the total band angular momentum. While this picture allows one to understand most of the properties of the system, it turns out to be insufficient for the description of hyperfine interactions in the valence band. In fact, the crystal symmetry allows a combination of p and d ($l = 2$) states in the valence band. This symmetry reduction opens the path to spin interactions that conserve the band angular momentum projections only modulo 2, thus enabling spin flip-flops between the heavy holes and nuclei, which would be forbidden by spin conservation in a system with full rotational symmetry [26,28]. Therefore, we include both p- and d-shell components in our model of atomic orbitals making up the valence band.

The scaling parameters ξ_s for the s-shell states are obtained from the experimentally determined values of the conduction band wave functions at the nucleus [42,43]. The distribution of the wave functions between the anion and cation is chosen to be consistent with the known experimental [42,43] and computational [27] data. In view of the lack of precise data, we choose $\xi_p = 0.85\xi_s$ for each atom, following the general relation between the scaling parameters of Slater orbitals [44–46] (neither the Slater orbitals themselves nor their scaling commonly used in tight-banding computations can be used directly, as they are optimized against chemical bonding and band structures and fail to reproduce the correct behavior near the nucleus). The d-shell scaling parameter ξ_d is estimated from the measured values of the hf coupling for holes [26] using the theoretically computed weights of d-shell admixtures in GaAs [27]. The resulting values of the parameters describing the hyperfine coupling are listed in Table I, where we also give the quantities $M_{ll'} = |\psi_s(0)|^{-2}\langle l|1/r^3|l'\rangle$ that characterize the geometry of the wave functions for the dipole hyperfine interaction. The details of the model are described in Ref. [28].

In view of the very small value of the nuclear Zeeman splitting, the probability for any nuclear configuration at thermal equilibrium is essentially the same at typical temperatures of

TABLE I. Nuclear [2] and atomic parameters.

	^{69}Ga	^{71}Ga	^{113}In	^{115}In	^{75}As
I	3/2	3/2	9/2	9/2	3/2
ζ	1.344	1.708	1.227	1.230	0.959
r	0.604	0.396	0.0428	0.9572	1
ξ_s	3.9		3.9		4.4
ξ_p	3.3		3.3		3.7
ξ_d	10.5		8.9		11.9
M_p	0.050		0.050		0.050
M_d	0.33		0.20		0.33
M_{sd}	0.048		0.034		0.049
$|\alpha_d|^2$	0.20		0.50		0.05
$|a_{C/A}^{cb}|^2$		0.50			0.50
$|a_{C/A}^{vb}|^2$		0.35			0.65

experiments involving self-assembled QDs (a few kelvins and above). Since the carrier Zeeman splitting is much larger than the nuclear one, the nuclear Zeeman energies can be neglected when considering the energy change in a carrier-nucleus spin flip-flop.

Coupling to phonons is described in the usual way. The phonon subsystem and the carrier-phonon interaction are described by the general Hamiltonian

$$H_{ph} = \sum_{\boldsymbol{k},\lambda}\hbar\omega_{\boldsymbol{k},\lambda}b_{\boldsymbol{k},\lambda}^\dagger b_{\boldsymbol{k},\lambda} + \sum_{\boldsymbol{k},\lambda}\{\Phi(\boldsymbol{r}),e^{i\boldsymbol{k}\cdot\boldsymbol{r}}\}(b_{\boldsymbol{k},\lambda} + b_{-\boldsymbol{k},\lambda}^\dagger),$$

where $\boldsymbol{k}$ and λ denote the wave vector and polarization of a phonon mode, respectively, $b_{\boldsymbol{k},\lambda}$ and $b_{-\boldsymbol{k},\lambda}^\dagger$ are the corresponding annihilation and creation operators, and $\Phi(\boldsymbol{r})$ is an 8×8 matrix of operators in the coordinate representation, corresponding to the eight-band structure of the $\boldsymbol{k}\cdot\boldsymbol{p}$ theory and accounting for deformation-potential and piezoelectric couplings. A detailed description of the carrier-phonon Hamiltonian is given in Ref. [47].

III. PHONON-ASSISTED SPIN-FLIP TRANSITIONS

In this section we present the theory for the phonon-assisted tunneling of carriers between the ground state manifolds of the two QDs with a simultaneous spin flip-flop between the carrier and a nuclear spin [Fig. 1(b)]. The eight-band $\boldsymbol{k}\cdot\boldsymbol{p}$ theory treats the electron and hole states on equal footing (the latter upon a standard transition from the electron picture of the completely filled valence band to the hole picture), and we present our theory for single-particle states in a general form, without specifying the kind of the carrier. In the following, the term "spin" is used to identify one of the two subbands of the conduction or heavy-hole valence band.

In a QDM structure with the two QDs separated by a relatively wide barrier, the single-particle wave functions are typically mostly localized in one of the QDs, with only a tail of the wave function extending to the other QD. If the energies of the ground states localized in the two QDs are close enough (separation smaller than the energy distance to the excited shells in each QD), then these two states built of the single-QD ground states (s shells) form the lowest molecular orbitals of the system, with energies further split

by the Zeeman effect in a magnetic field. Here we will work in such a parameter range. A particular situation occurs where the ground states of the two QDs are energetically aligned. Then, the two molecular orbitals become delocalized between the two QDs and take the form of bonding and antibonding orbitals with wave functions that are approximately even or odd along the growth axis, respectively. The minimum energy splitting at such a resonance is a measure of tunnel coupling between the QDs [31].

In order to find the rate for a spin flip-flop process between the two lowest states described above, we first calculate the hyperfine flip-flop correction to the system state. We denote the carrier state in the nth QD ($n = 1, 2$) with the nominal spin orientation σ (resulting from the $\mathbf{k} \cdot \mathbf{p}$ diagonalization) by $|n\sigma\rangle$ and its energy by $E_\sigma^{(n)}$. The state of the nuclei is labeled by $|\cdots m_\alpha \cdots\rangle$, where m_α is the quantum number for the z projection of the respective nuclear spin. The states unperturbed by the hyperfine coupling are of a product form $|n\sigma; \cdots m_\alpha \cdots\rangle = |n\sigma\rangle \otimes |\cdots m_\alpha \cdots\rangle$. We restrict our theory to the case of sufficiently strong tunnel coupling between the QDs, such that the Zeeman energy is small compared to the energy splitting between the two lowest molecular orbitals, which is the case for all the results shown here (a more general theory would be needed only for holes in fields $B \gtrsim 1$ T and very close to the exact tunneling resonance). In the lowest order of perturbation theory with respect to the hyperfine interaction the eigenstates of the system are then

$$|\Psi_{n\sigma; \cdots m_\alpha \cdots}\rangle = |n\sigma; \cdots m_\alpha \cdots\rangle + \sum_\alpha c_{\alpha+}^{(n\sigma)} |n\overline{\sigma}; \cdots m_\alpha + 1 \cdots\rangle$$
$$+ \sum_\alpha c_{\alpha-}^{(n\sigma)} |n\overline{\sigma}; \cdots m_\alpha - 1 \cdots\rangle, \quad (3)$$

where $\overline{\sigma}$ denotes inverted spin and the nuclear configuration on the right-hand side is the same as the one on the left-hand side except for the one explicitly given modified spin. The coefficients of the perturbative correction are

$$c_{\alpha\pm}^{(n\sigma)} = \frac{\langle n\overline{\sigma}; \cdots m_\alpha \pm 1 \cdots |H_{\mathrm{hf}}|n\sigma; \cdots m_\alpha \cdots\rangle}{\hbar\omega_{\sigma\overline{\sigma}}^{(nn)}}$$
$$= \frac{3E_{\mathrm{hf}}\zeta_\alpha}{2\hbar\omega_{\sigma\overline{\sigma}}^{(nn)}} \sqrt{j(j+1) - m_\alpha(m_\alpha \pm 1)} \langle n\overline{\sigma}|A_\mp^{(\alpha)}|n\sigma\rangle,$$

where $A_\pm^{(\alpha)} = A_x(\mathbf{r} - \mathbf{R}_\alpha) \pm iA_y(\mathbf{r} - \mathbf{R}_\alpha)$ and $\omega_{\sigma\sigma'}^{(nn')} = (E_\sigma^{(n)} - E_{\sigma'}^{(n')})/\hbar$. The matrix elements of $A_\pm^{(\alpha)}$ are calculated using the model of Bloch functions described in Sec. II and following the multiband approach developed in Ref. [28]. In the short-range approximation [22,23,48,49], these operators are localized on the nucleus α, which leads to the physically obvious property that the largest contribution comes from the nuclei at which the probability density for the state n is the largest.

From Fermi's golden rule, the probability of a phonon-assisted transition from the state with spin σ in QD1 to the state with spin σ' in QD2 with a change in the nuclear configuration from $\{m_\alpha\}$ to $\{m_\alpha'\}$ is

$$\Gamma_{\sigma\to\sigma'}^{\{m_\alpha\}\to\{m_\alpha'\}} = \frac{2\pi}{\hbar}|n_{\mathrm{B}}(\omega_{\sigma\sigma'}^{(12)}) + 1| \sum_{\mathbf{k},\lambda} \delta(\hbar\omega_{\mathbf{k},\lambda} - |\omega_{\sigma\sigma'}^{(12)}|)$$
$$\times |\langle\Psi_{2\sigma'; \cdots m_\alpha' \cdots}|\{\Phi(\mathbf{r}), e^{i\mathbf{k}\cdot\mathbf{r}}\}|\Psi_{1\sigma; \cdots m_\alpha \cdots}\rangle|^2.$$

Substituting the perturbation expansion from Eq. (3), taking into account the obvious fact that the phonon interaction conserves nuclear spins, and denoting

$$F_{\sigma'\sigma}(\mathbf{k}) = \langle 2\sigma'|\{\Phi(\mathbf{r}), e^{i\mathbf{k}\cdot\mathbf{r}}\}|1\sigma\rangle, \quad (4)$$

one finds

$$\langle\Psi_{2\sigma'; \cdots m_\alpha' \cdots}|\{\Phi(\mathbf{r}), e^{i\mathbf{k}\cdot\mathbf{r}}\}|\Psi_{1\sigma; \cdots m_\alpha \cdots}\rangle$$
$$= F_{\sigma'\sigma}(\mathbf{k}) + F_{\sigma'\overline{\sigma}}(\mathbf{k}) \sum_{\alpha,\pm} c_{\alpha\pm}^{(1\sigma)} \langle \cdots m_\alpha' \cdots | \cdots m_\alpha \pm 1 \cdots\rangle$$
$$+ F_{\overline{\sigma'}\sigma}(\mathbf{k}) \sum_{\alpha,\pm} c_{\alpha\pm}^{(2\sigma')*} \langle \cdots m_\alpha' \pm 1 \cdots | \cdots m_\alpha \cdots\rangle + \cdots. \quad (5)$$

Since the multiband carrier wave functions are dominated by one leading component (determining the nominal "spin" of the state), the couplings $F_{\sigma'\sigma}(\mathbf{k})$ are large for $\sigma = \sigma'$ and much smaller otherwise, when they stem from the band mixing involving SO couplings. The hyperfine admixture amplitudes $c_{\alpha\pm}^{(n\sigma)}$ are small as well. Therefore, in Eq. (5) we kept only the contributions in the leading order in the SO or hf couplings, neglecting those relying on both these weak couplings simultaneously. Furthermore, for a nominally spin-conserving process ($\sigma = \sigma'$), the transition amplitude is by far dominated by the first contribution $F_{\sigma\sigma}(\mathbf{k})$, which determines the spin-conserving phonon-assisted tunneling rate

$$\Gamma_{\sigma\to\sigma} = 2\pi R_{\sigma\sigma\sigma\sigma}(|\omega_{\sigma\sigma}^{(12)}|), \quad (6)$$

where we define the spectral densities for the phonon bath as

$$R_{\sigma_1\sigma_2\sigma_3\sigma_4}(\omega) = \frac{1}{\hbar^2}|n_{\mathrm{B}}(\omega) + 1|$$
$$\times \sum_{\mathbf{k},\lambda} F_{\sigma_1\sigma_2}(\mathbf{k})F_{\sigma_4\sigma_3}^*(\mathbf{k})\delta(\omega_{\mathbf{k},\lambda} - |\omega|). \quad (7)$$

For a spin-flip process, there are two mechanisms that may, in principle, yield comparable contributions: the SO channel entering via the first term and the hyperfine channel accounted for by the two other terms on the right-hand side of Eq. (5). The total spin-flip transition rate is then a sum of the SO rate,

$$\Gamma_{\sigma\to\overline{\sigma}}^{(\mathrm{so})} = 2\pi R_{\sigma\overline{\sigma}\sigma\sigma}(\omega_{\sigma\overline{\sigma}}^{(12)}), \quad (8)$$

and the rates for hyperfine transitions, summed up over final configurations of the nuclear bath, differing by one nuclear spin flip from the initial one,

$$\Gamma_{\sigma\to\overline{\sigma}}^{(\mathrm{hf})}(\cdots m_\alpha \cdots) = \sum_\alpha \Gamma_{\sigma\to\overline{\sigma}}^{(\mathrm{hf}),\alpha}(\cdots m_\alpha \cdots), \quad (9)$$

where we explicitly note the dependence on the initial configuration of the nuclear bath and

$$\Gamma_{\sigma\to\overline{\sigma}}^{(\mathrm{hf}),\alpha}(\cdots m_\alpha \cdots) = 2\pi \sum_{a=\sigma,\overline{\sigma}} \sum_{b=\sigma,\overline{\sigma}} Q_{ab}^{(\alpha)} R_{aabb}(\omega_{\sigma\overline{\sigma}}^{(12)}), \quad (10)$$

with

$$Q_{\sigma\sigma}^{(\alpha)} = \left(\frac{3E_{\text{hf}}\zeta_\alpha}{2\hbar\omega_{\overline{\sigma}\sigma}^{(22)}}\right)^2 \{[j(j+1) - m_\alpha(m_\alpha - 1)]|\langle 2\sigma|A_-^{(\alpha)}|2\overline{\sigma}\rangle|^2 + [j(j+1) - m_\alpha(m_\alpha + 1)]|\langle 2\sigma|A_+^{(\alpha)}|2\overline{\sigma}\rangle|^2\},$$

$$Q_{\overline{\sigma}\overline{\sigma}}^{(\alpha)} = \left(\frac{3E_{\text{hf}}\zeta_\alpha}{2\hbar\omega_{\sigma\overline{\sigma}}^{(11)}}\right)^2 \{[j(j+1) - m_\alpha(m_\alpha + 1)]|\langle 1\overline{\sigma}|A_-^{(\alpha)}|1\sigma\rangle|^2 + [j(j+1) - m_\alpha(m_\alpha - 1)]|\langle 1\overline{\sigma}|A_+^{(\alpha)}|1\sigma\rangle|^2\},$$

$$Q_{\overline{\sigma}\sigma}^{(\alpha)} = Q_{\sigma\overline{\sigma}}^{(\alpha)*} = \frac{(3E_{\text{hf}}\zeta_\alpha)^2}{4\hbar^2\omega_{\sigma\overline{\sigma}}^{(11)}\omega_{\overline{\sigma}\sigma}^{(22)}}\{[j(j+1) - m_\alpha(m_\alpha + 1)]\langle 1\overline{\sigma}|A_-^{(\alpha)}|1\sigma\rangle\langle 2\sigma|A_+^{(\alpha)}|2\overline{\sigma}\rangle$$

$$+ [j(j+1) - m_\alpha(m_\alpha - 1)]\langle 1\overline{\sigma}|A_+^{(\alpha)}|1\sigma\rangle\langle 2\sigma|A_-^{(\alpha)}|2\overline{\sigma}\rangle\}.$$

Note that $R_{\sigma\sigma\overline{\sigma}\overline{\sigma}}(\omega) = R_{\overline{\sigma}\overline{\sigma}\sigma\sigma}^*(\omega)$, so $\Gamma_{\sigma\to\overline{\sigma}}^{(\text{hf}),\alpha}$ is real.

Since the shape of the wave function for a given spatial state in a given QD very weakly depends on the spin orientation, all the spectral densities in Eq. (10) are almost identical upon an appropriate choice of the arbitrary phases. This allows one to write

$$\Gamma_{\sigma\to\overline{\sigma}}^{(\text{hf}),\alpha}(\cdots m_\alpha \cdots) = 2\pi R\big(\omega_{\sigma\overline{\sigma}}^{(12)}\big) \sum_{a=\sigma,\overline{\sigma}} \sum_{b=\sigma,\overline{\sigma}} Q_{ab}^{(\alpha)}$$

$$= 2\pi R\big(\omega_{\sigma\overline{\sigma}}^{(12)}\big)\frac{(3E_{\text{hf}}\zeta_\alpha)^2}{4}\{[j(j+1) - m_\alpha(m_\alpha + 1)]|\langle 2\sigma|A_+^{(\alpha)}|2\overline{\sigma}\rangle - \langle 1\sigma|A_+^{(\alpha)}|1\overline{\sigma}\rangle|^2$$

$$+ [j(j+1) - m_\alpha(m_\alpha - 1)]|\langle 2\sigma|A_-^{(\alpha)}|2\overline{\sigma}\rangle - \langle 1\sigma|A_-^{(\alpha)}|1\overline{\sigma}\rangle|^2\}. \tag{11}$$

For a transition between the Zeeman states in a single QD the wave functions of states 1 and 2 are nearly the same; hence, the two matrix elements of $A_\pm^{(\alpha)}$ in Eq. (11) become identical, and the transition rate is suppressed by destructive interference. Therefore, the contribution of the hf transitions to spin relaxation in this case relies on higher state admixture, shows a higher-order field dependence (which may be related to Van Vleck cancellation due to time reversal symmetry like in the SO case [50]), and is therefore limited to magnetic fields below 1 T even for electrons [51]. This single-QD situation is shown in graphical form in Fig. 2(a), where the process involving a selected nuclear spin is represented as a transition via a virtual state, splitting the phonon-assisted hf flip-flop into the hf and phonon-induced (ph) transitions. Both quantum amplitudes for the two paths have the same absolute value but different phases, leading to destructive interference. In contrast, in the QDM system, as long as the states are spatially separated (away from the level-crossing resonance at which the ground states in the two QDs are aligned), each nucleus is effectively coupled to at most one carrier state (the one localized in the same QD as the nucleus), and only one of the two interfering amplitudes can be large. As shown in Fig. 2(b), depending on the localization of the flipped nuclear spin in the "initial" or "final" QD, either the ph-hf or hf-ph sequence has a large amplitude, while the other one is suppressed due to weak overlap between the nucleus and the carrier wave function. From this graphical representation it is also clear that the relaxation can involve a nuclear spin in one or the other QD with a similar probability.

For unpolarized nuclei the physically meaningful rate is obtained by averaging Eq. (9) over all the initial configurations of the nuclear spins and summing up over all nuclear spin flips,

$$\overline{\Gamma}_{\sigma\to\overline{\sigma}}^{(\text{hf})} = 2\pi \sum_{a=\sigma,\overline{\sigma}} \sum_{b=\sigma,\overline{\sigma}} \overline{Q}_{ab} R_{aabb}\big(\omega_{\sigma\overline{\sigma}}^{(12)}\big). \tag{12}$$

Since $\langle j(j+1) - m_\alpha(m_\alpha \pm 1)\rangle = 2j(j+1)/3$, one finds

$$\overline{Q}_{\sigma\sigma} = \sum_\alpha \left(\frac{3E_{\text{hf}}\zeta_\alpha}{2\hbar\omega_{\overline{\sigma}\sigma}^{(22)}}\right)^2 \frac{2j(j+1)}{3}$$

$$\times (|\langle 2\sigma|A_-^{(\alpha)}|2\overline{\sigma}\rangle|^2 + |\langle 2\sigma|A_+^{(\alpha)}|2\overline{\sigma}\rangle|^2), \tag{13a}$$

$$\overline{Q}_{\overline{\sigma}\overline{\sigma}} = \sum_\alpha \left(\frac{3E_{\text{hf}}\zeta_\alpha}{2\hbar\omega_\sigma\overline{\sigma}^{(11)}}\right)^2 \frac{2j(j+1)}{3}$$

$$\times (|\langle 1\overline{\sigma}|A_-^{(\alpha)}|1\sigma\rangle|^2 + |\langle 1\overline{\sigma}|A_+^{(\alpha)}|1\sigma\rangle|^2), \tag{13b}$$

$$\overline{Q}_{\overline{\sigma}\sigma} = \overline{Q}_{\sigma\overline{\sigma}}^* = \sum_\alpha \frac{(3E_{\text{hf}}\zeta_\alpha)^2}{4\hbar^2\omega_{\sigma\overline{\sigma}}^{(11)}\omega_{\overline{\sigma}\sigma}^{(22)}} \frac{2j(j+1)}{3}$$

$$\times (\langle 1\overline{\sigma}|A_-^{(\alpha)}|1\sigma\rangle\langle 2\sigma|A_+^{(\alpha)}|2\overline{\sigma}\rangle$$

$$+ \langle 1\overline{\sigma}|A_+^{(\alpha)}|1\sigma\rangle\langle 2\sigma|A_-^{(\alpha)}|2\overline{\sigma}\rangle). \tag{13c}$$

IV. RESULTS

In this section we analyze and compare the electron and hole phonon-assisted tunneling rates with hyperfine- and SO-induced spin flips, as well as the spin-conserving tunneling rates. The rates are calculated using Eq. (12), corresponding to the thermal equilibrium of the nuclear bath at temperatures much higher than the nuclear Zeeman energies. The matrix elements in Eqs. (13) are evaluated using the $\boldsymbol{k}\cdot\boldsymbol{p}$ formalism for hyperfine interactions developed in our previous paper [28], while the spectral densities are computed directly from the $\boldsymbol{k}\cdot\boldsymbol{p}$ wave functions according to the definitions in Eqs. (4) and (7).

Before discussing the relaxation rates, let us briefly summarize the typical energies in our system in order to validate the model. Obviously, the critical parameter area is the vicinity of the tunnel resonance, where the energy splitting between
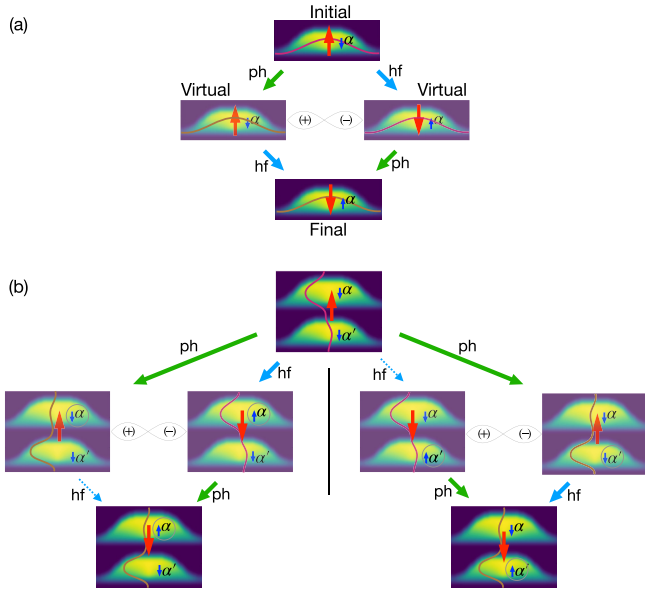
FIG. 2. Phonon-assisted hf relaxation as a transition via an intermediate virtual state. (a) Transition within the ground-state Zeeman doublet in a single QD; (b) transition between the two states forming the ground state manifold of a QDM. The magenta and brown curves schematically represent the wave functions of the initial and final states, respectively. The red arrow is the electron spin. The blue arrows show spins of representative nuclei. The hf and phonon-induced transitions are represented by blue and green arrows, while the dotted arrow marks a hf transition that is inefficient due to small wave function overlap.
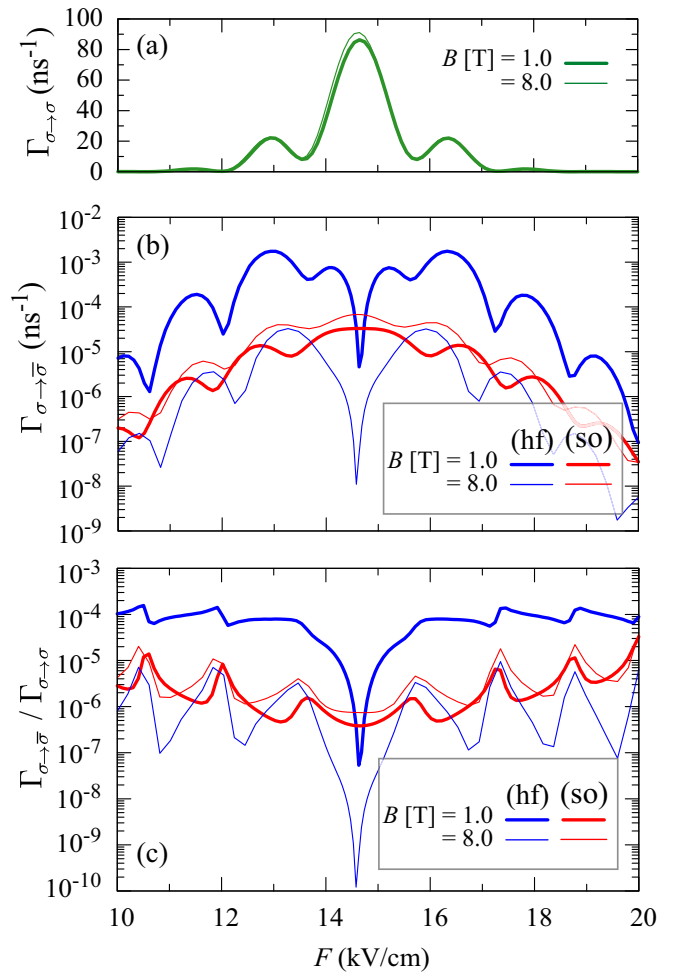

FIG. 3. (a) Spin-conserving phonon-assisted tunneling rate of an electron at two values of the magnetic field as a function of the axial electric field. (b) Spin-flip transition rates due the hf (blue lines) and SO (red lines) interaction. (c) Ratio of the spin-flip to the spin-conserving phonon-assisted tunneling rates for both transition channels.

the two lowest molecular orbitals is the smallest. For the structure under consideration, the minimum splitting between these orbitals is 1.4 and 0.08 meV for electrons and holes, respectively. The Zeeman splitting for electrons is 0.06 meV at $B = 1$ T; hence, it is smaller than the tunnel splitting between the molecular states in a wide range of magnetic fields, as assumed in our model. On the other hand, we find the hole Zeeman splitting of 0.012 meV at $B = 0.1$ T. Therefore, at fields on the order of 1 T it becomes comparable to the tunnel splitting, and the model ceases to be valid in a narrow range of electric fields around the resonance. We do not refer to this parameter range in our discussion.

Figure 3(a) shows the spin-conserving relaxation rates between the two lowest electron states as a function of the electric field F applied in the growth direction z that relatively shifts the ground state manifolds of the two QDs. The results are shown at two values of the magnetic field oriented along the growth direction (Faraday configuration). The central maximum corresponds to the tunneling resonance when the two levels are aligned and form an anticrossing. The oscillations are due to the interplay between the QD separation and the wavelength of the emitted phonon as the energy splitting between the two levels is changed [52]. The difference between the relaxation rates at the two values of magnetic field is marginal.

In Fig. 3(b) we show the spin-flip tunneling rates for the electron in the presence of electric and magnetic fields as in Fig. 3(a), comparing the rates calculated according to the

theory presented above with those resulting from the SO couplings [53]. The oscillations visible in Fig. 3(b) have the same geometrical origin as those in Fig. 3(a). At weak magnetic fields (here we choose $B = 1$ T) the hyperfine channel dominates over the spin-orbit one. On the other hand, for moderate and strong values of magnetic field (here $B = 8.0$ T), the spin-flip transitions caused by the SO couplings are stronger due to the very different magnetic field dependences of these two classes of transitions. The hf transition relies on the admixture of the spin-flipped state, which can be treated within the lowest-order perturbation theory, as described by Eq. (3). The admixed state involves a flipped nucleus and the Zeeman companion of the initial or final state. Neglecting the nuclear Zeeman energy, the lowest-order perturbative coefficients $c_{\alpha\pm}^{(n\sigma)}$ are therefore inversely proportional to the carrier Zeeman splitting and therefore vary as $1/B$, leading to the $\propto 1/B^2$ dependence of the hf rate. On the other hand, the rate of the SO relaxation increases slowly in the considered range of the magnetic fields, in contrast to the relaxation within the Zeeman doublet, where a strong power-law dependence

is observed. This absence of the power-law increase is due to the fact that neither of the reasons for the typical B^5 dependence in single QDs [32,54] (the dependence of the energy splitting and time-reversal symmetry between the initial and final states) holds here [53]. As a result, the SO relaxation rate remains finite at zero magnetic field, and in the particular structure studied here it grows rather slowly with B.

In the case of the hyperfine-induced transitions, we observe a minimum at the field value corresponding to the resonance condition (crossing of the ground states of the two QDs). Under such conditions both wave functions are delocalized over the two QDs; the discrimination of the two paths in Fig. 2(b) is suppressed, and a destructive interference of the two matrix elements of $A_\pm$ in Eq. (11) takes place. In our case (and typically for self-assembled QDMs in general in weak and moderate magnetic fields) the coupling energy is larger than the Zeeman energy; hence, different spatial states with opposite spins do not cross near the resonance. Such a crossing might occur for very weakly coupled QDs, leading to a different behavior. In such a case, phonon-assisted processes would be suppressed due to low spectral density at low-energy splittings, and the tunneling would rely on energy-conserving flip-flops, which may be enabled by quadrupole broadening.

The ratio of spin-flip to spin-conserving transition rates is shown in Fig. 3(c). This value is equal to the probability of spin flip during the incoherent phonon-assisted tunneling and therefore is a measure of spin preservation in this process. Typical values are on the order of 10^{-4} at 1 T, dominated by the hf coupling and scaling as $1/B^2$ at lower fields, while at higher fields the spin-flip process is dominated by the SO coupling, and its probability is reduced to 10^{-6}. The oscillations of these rates as a function of the electric field result from the interplay between the patterns of oscillations of the spin-conserving and two spin-flip rates. These patterns are not identical for a few reasons. First, the spin-flip transition is associated with a slightly different energy transfer and hence phonon wavelength. Second, the transitions couple to different phonon modes. Third, the oscillations are modulated by an envelope which decays in different ways, which shifts the maxima and minima. Altogether, the spin-conserving and spin-flip rates do not oscillate strictly proportionally, which results in oscillations of their ratio.

The results for a hole are presented in Fig. 4. Again, we show the electric field dependence of the spin-flip rate for the two spin relaxation mechanisms at two magnitudes of the magnetic field. For a hole, the spin-conserving phonon-assisted relaxation, shown in Fig. 4(a), is slower than for an electron due to weaker deformation potential coupling [31]. In addition, when the states are localized in different QDs, the phonon-assisted tunneling is less efficient because of the higher hole mass and hence stronger localization.

For a hole, as can be seen in Fig. 4(b), the two spin-flip channels depend in different ways on the energy splitting controlled by the external electric field. As a result, at a given magnetic field, one or the other process may dominate. In the vicinity of the resonance, when the phonon-assisted relaxation or tunneling process is effective, the cross-over between the two mechanisms occurs at magnetic field amplitudes of a fraction of Tesla, much lower than in the case of an electron.
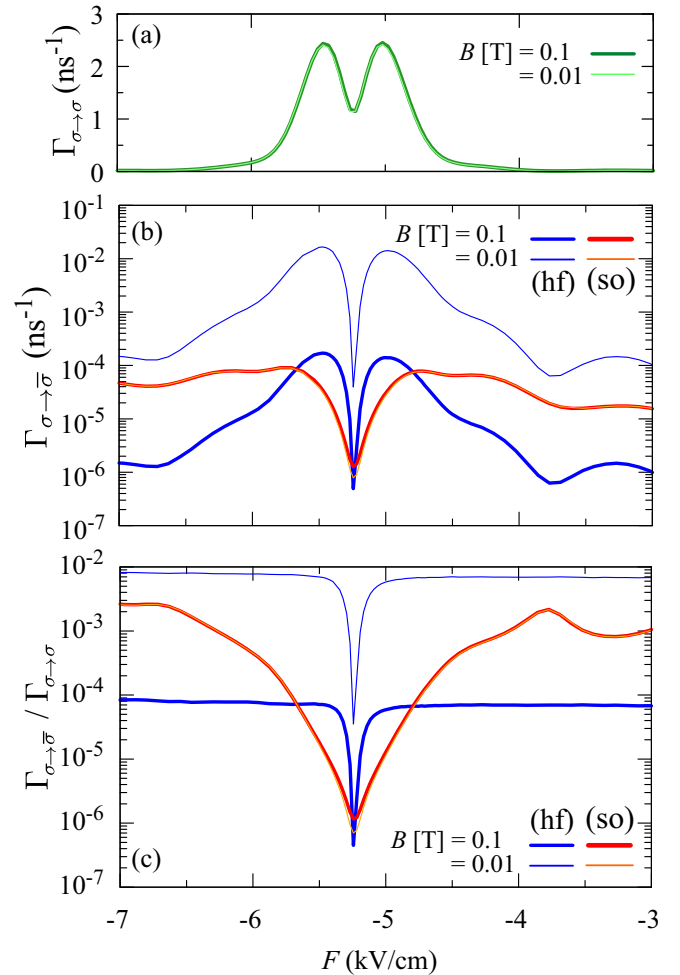

FIG. 4. (a) Spin-conserving phonon-assisted tunneling rate of a hole. (b) Spin-flip transition rates related to the hf (blue lines) and SO (red lines) coupling. (c) Ratio of the spin flip to the spin-conserving phonon-assisted process for both transition channels.

This is due to the fact that the hyperfine-induced spin flip is much less probable than for an electron as a consequence of the much lower hf coupling for holes, while the SO-induced process is a few times more effective. Here the SO channel is nearly magnetic-field-independent (again in contrast to the relaxation between Zeeman sublevels [17,39] for the same reasons as explained above for the electron), while the rate for the hf channel scales as $1/B^2$.

The spin-flip probability, given by the ratio of the spin-conserving to spin-flip rates [Fig. 4(c)], is dominated by the hf-induced process at very low fields, on the order of 0.01 T and below, with a remarkably high probability of the spin flip on the order of 1% at $B = 0.01$ T except in the closest vicinity of the resonance. At higher fields the importance of this process is reduced, leading to a much lower relative efficiency of the spin-flip process near the resonance, while far away from the resonance the increasing SO contribution yield overall probabilities on the order of 10^{-3}.

In Fig. 5 we present the crossover between the SO and hf-dominated hole spin flip as a function of the magnetic field at an electric field magnitude of $F = -5$ kV/cm, near
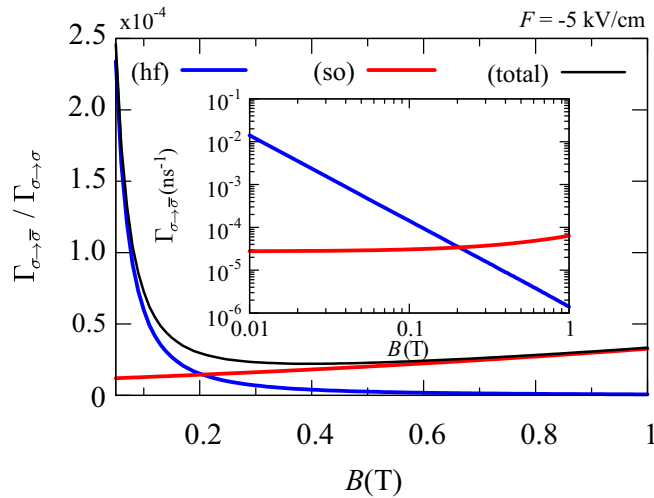
FIG. 5. Spin-flip relaxation rates for a hole for the two spin-flip channels as a function of the magnetic field for a fixed electric field $F = -5$ kV/cm. The relative spin-flip rates (the spin-flip probabilities) for the two channels along with the total relative rate. Inset: The absolute spin-flip relaxation rates for the two mechanisms.

the maximum of the relaxation rate (this time using a linear scale). At this electric field value the crossover takes place at $B \approx 0.2$ T (the exact value obviously depends on the electric field). While the hf channel manifests the $1/B^2$ dependence visible already in Fig. 4, the SO contribution shows a very weak increase with the magnetic field (see the inset in Fig. 5), which was not noticeable earlier. As a result, the total relative spin-flip rate (spin-flip probability) is a nonmonotonic function of the magnetic field over an experimentally accessible range of field magnitudes. A similar nonmonotonic dependence holds for an electron, similar to the relaxation within the Zeeman doublet in a single QD, where such a crossover was recently observed [51]. In our case, depending on the value of the electric field, the minimum for the electron is less pronounced and shifted to higher magnetic fields (well above the SO-hf crossover) or even absent due to weaker magnetic field dependence of the SO component for electrons, which in some cases may even decrease at higher magnetic fields.

V. CONCLUSIONS

We have calculated the rates of phonon-assisted hyperfine and spin-orbit-induced spin flips during electron and hole relaxation in a self-assembled QDM using a multiband theory of hyperfine couplings based on the $\mathbf{k} \cdot \mathbf{p}$ model. We have predicted a crossover between the two processes as dominant spin-flip mechanisms at magnetic fields of a few teslas and on the order of 0.1 T for electrons and holes, respectively, with the hf mechanism scaling as $1/B^2$ and dominating at lower fields over the nearly magnetic field independent SO channel. For the QDM structure considered here, the probability of spin flip during electron tunneling between the QDs can be large at low fields (about 1% for electrons and holes at magnetic fields of 0.1 and 0.01 T, respectively) but decreases strongly with increasing field, reaching values around 10^{-6} and 10^{-4} for electrons and holes, respectively, when the SO coupling dominates the relaxation.

The interplay between the two channels with opposite magnetic field dependences of the relative spin-flip rates leads to a nonmonotonic dependence of the total relative spin-flip rate. The resulting minimum is particularly pronounced for holes and could be observed in the spin-flip tunneling process, in contrast to spin relaxation within the Zeeman doublet, where the hyperfine effects are limited to much lower fields and are probably not visible for holes. This prediction relies on the assumed strong transverse hf coupling for holes, in line with some recent experiments and with theoretical predictions based on the d-shell admixture to the valence band states. As the spin-flip efficiency is, in principle, measurable in optical experiments, this prediction might be used for testing the presence of the transverse hf couplings. Another interesting field of further study is the singlet-triplet relaxation of two-electron systems in QDMs [30,55,56].

ACKNOWLEDGMENTS

[1] M. M. Glazov, *Electron and Nuclear Spin Dynamics in Semiconductor Nanostructures* (Oxford University Press, Oxford, 2018).

[2] J. Schliemann, A. Khaetskii, and D. Loss, J. Phys.: Condens. Matter **15**, R1809(R) (2003).

[3] W. A. Coish and J. Baugh, Phys. Status Solidi B **246**, 2203 (2009).

[4] Ł. Cywiński, Acta Phys. Pol. A **119**, 576 (2011).

[5] B. Urbaszek, X. Marie, T. Amand, O. Krebs, P. Voisin, P. Maletinsky, A. Högele, and A. Imamoğlu, Rev. Mod. Phys. **85**, 79 (2013).

[6] E. A. Chekhovich, A. B. Krysa, M. S. Skolnick, and A. I. Tartakovskii, Phys. Rev. Lett. **106**, 027402 (2011).

[7] D. S. Smirnov, T. S. Shamirzaev, D. R. Yakovlev, and M. Bayer, Phys. Rev. Lett. **125**, 156801 (2020).

[8] E. A. Chekhovich, S. F. C. da Silva, and A. Rastelli, Nat. Nanotechnol. **15**, 999 (2020).

[9] A. M. Waeber, G. Gillard, G. Ragunathan, M. Hopkinson, P. Spencer, D. A. Ritchie, M. S. Skolnick, and E. A. Chekhovich, Nat. Commun. **10**, 3157 (2019).

[10] B. Eble, C. Testelin, P. Desfonds, F. Bernardot, A. Balocchi, T. Amand, A. Miard, A. Lemaître, X. Marie, and M. Chamarro, Phys. Rev. Lett. **102**, 146601 (2009).

[11] X. M. Dou, B. Q. Sun, D. S. Jiang, H. Q. Ni, and Z. C. Niu, J. Appl. Phys. **111**, 053524 (2012).

[12] F. Fras, B. Eble, P. Desfonds, F. Bernardot, C. Testelin, M. Chamarro, A. Miard, and A. Lemaître, Phys. Rev. B **86**, 045306 (2012).

[13] H. Kurtze, D. R. Yakovlev, D. Reuter, A. D. Wieck, and M. Bayer, Phys. Rev. B **85**, 195303 (2012).

[14] P.-F. Braun, X. Marie, L. Lombez, B. Urbaszek, T. Amand, P. Renucci, V. K. Kalevich, K. V. Kavokin, O. Krebs, P. Voisin, and Y. Masumoto, Phys. Rev. Lett. **94**, 116601 (2005).

[15] P. Glasenapp, D. S. Smirnov, A. Greilich, J. Hackmann, M. M. Glazov, F. B. Anders, and M. Bayer, Phys. Rev. B **93**, 205429 (2016).

[16] J. Beyer, Y. Puttisong, I. A. Buyanova, S. Suraprapapich, C. W. Tu, and W. M. Chen, Appl. Phys. Lett. **100**, 143105 (2012).

[17] D. Heiss, S. Schaeck, H. Huebl, M. Bichler, G. Abstreiter, J. J. Finley, D. V. Bulaev, and D. Loss, Phys. Rev. B **76**, 241306(R) (2007).

[18] D. V. Bulaev and D. Loss, Phys. Rev. Lett. **95**, 076805 (2005).

[19] L. C. Camenzind, L. Yu, P. Stano, J. D. Zimmerman, A. C. Gossard, D. Loss, and D. M. Zumbühl, Nat. Commun. **9**, 3454 (2018).

[20] S. I. Erlingsson and Y. V. Nazarov, Phys. Rev. B **66**, 155327 (2002).

[21] S. I. Erlingsson and Y. V. Nazarov, Phys. Rev. B **70**, 205327 (2004).

[22] J. Fischer, W. A. Coish, D. V. Bulaev, and D. Loss, Phys. Rev. B **78**, 155329 (2008).

[23] C. Testelin, F. Bernardot, B. Eble, and M. Chamarro, Phys. Rev. B **79**, 195440 (2009).

[24] P. Fallahi, S. T. Yılmaz, and A. Imamoğlu, Phys. Rev. Lett. **105**, 257402 (2010).

[25] J. H. Prechtel, A. V. Kuhlmann, J. Houel, A. Ludwig, S. R. Valentin, R. J. Warburton, A. D. Wieck, and R. J. Warburton, Nat. Mater. **15**, 981 (2016).

[26] E. A. Chekhovich, M. M. Glazov, A. B. Krysa, M. Hopkinson, P. Senellart, A. Lemaître, M. S. Skolnick, and A. I. Tartakovskii, Nat. Phys. **9**, 74 (2013).

[27] P. Boguslawski and I. Gorczyca, Semicond. Sci. Technol. **9**, 2169 (1994).

[28] P. Machnikowski, K. Gawarecki, and Ł. Cywiński, Phys. Rev. B **100**, 085305 (2019).

[29] Y. Sato, J. C. H. Chen, M. Hashisaka, K. Muraki, and T. Fujisawa, Phys. Rev. B **96**, 115416 (2017).

[30] S. Matsuo, K. Kuroyama, S. Yabunaka, S. R. Valentin, A. Ludwig, A. D. Wieck, and S. Tarucha, Phys. Rev. Res. **2**, 033120 (2020).

[31] K. Gawarecki and P. Machnikowski, Phys. Rev. B **85**, 041305(R) (2012).

[32] A. Mielnik-Pyszczorski, K. Gawarecki, M. Gawełczyk, and P. Machnikowski, Phys. Rev. B **97**, 245313 (2018).

[33] P.-L. Ardelt, M. Koller, T. Simmet, L. Hanschke, A. Bechtold, A. Regler, J. Wierzbowski, H. Riedl, J. J. Finley, and K. Müller, Phys. Rev. B **93**, 165305 (2016).

[34] V. Jovanov, T. Eissfeller, S. Kapfinger, E. C. Clark, F. Klotz, M. Bichler, J. G. Keizer, P. M. Koenraad, M. S. Brandt, G. Abstreiter, and J. J. Finley, Phys. Rev. B **85**, 165433 (2012).

[35] C. Pryor, J. Kim, L. W. Wang, A. J. Williamson, and A. Zunger, J. Appl. Phys. **83**, 2548 (1998).

[36] G. Bester, X. Wu, D. Vanderbilt, and A. Zunger, Phys. Rev. Lett. **96**, 187602 (2006).

[37] M. A. Caro, S. Schulz, and E. P. O'Reilly, Phys. Rev. B **91**, 075203 (2015).

[38] K. Gawarecki, Phys. Rev. B **97**, 235408 (2018).

[39] M. Krzykowski, K. Gawarecki, and P. Machnikowski, Phys. Rev. B **102**, 205301 (2020).

[40] C.-W. Huang and X. Hu, Phys. Rev. B **81**, 205304 (2010).

[41] C. Latta, A. Srivastava, and A. Imamoğlu, Phys. Rev. Lett. **107**, 167401 (2011).

[42] E. A. Chekhovich, A. Ulhaq, E. Zallo, F. Ding, O. G. Schmidt, and M. S. Skolnick, Nat. Mater. **16**, 982 (2017).

[43] M. Gueron, Phys. Rev. **135**, A200 (1964).

[44] E. Clementi and D. L. Raimondi, J. Chem. Phys. **38**, 2686 (1963).

[45] E. Clementi, J. Chem. Phys. **47**, 1300 (1967).

[46] R. Benchamekh, F. Raouafi, J. Even, F. Ben Cheikh Larbi, P. Voisin, and J.-M. Jancu, Phys. Rev. B **91**, 045118 (2015).

[47] K. Gawarecki and M. Krzykowski, Phys. Rev. B **99**, 125401 (2019).

[48] Y. Obata, J. Phys. Soc. Jpn. **18**, 1020 (1963).

[49] E. B. Hale and R. L. Mieher, Phys. Rev. B **3**, 1955 (1971).

[50] A. V. Khaetskii and Y. V. Nazarov, Phys. Rev. B **64**, 125316 (2001).

[51] G. Gillard, I. M. Griffiths, G. Ragunathan, A. Ulhaq, C. McEwan, E. Clarke, and E. A. Chekhovich, npj Quantum Inf. **7**, 43 (2021).

[52] K. Gawarecki, M. Pochwała, A. Grodecka-Grad, and P. Machnikowski, Phys. Rev. B **81**, 245312 (2010).

[53] M. Gawełczyk and K. Gawarecki, Phys. Rev. B **103**, 245422 (2021).

[54] M. Kroutvar, Y. Ducommun, D. Heiss, M. Bichler, D. Schuh, G. Abstreiter, and J. J. Finley, Nature (London) **432**, 81 (2004).

[55] J. Danon, Phys. Rev. B **88**, 075306 (2013).

[56] F. R. Braakman, J. Danon, L. R. Schreiber, W. Wegscheider, and L. M. K. Vandersypen, Phys. Rev. B **89**, 075417 (2014).

[57] http://wcss.pl.